

Research Article

Evaluation of Diversity Antenna Designs Using Ray Tracing, Measured Radiation Patterns, and MIMO Channel Measurements

Arindam Pal, Chris Williams, Geoff Hilton, and Mark Beach

Centre for Communications Research, University of Bristol, Bristol BS8 1UB, UK

Received 31 March 2006; Revised 11 September 2006; Accepted 23 October 2006

Recommended by Mérouane Debbah

This paper presents an evaluation of the MIMO performance of three candidate antenna array designs, each embedded within a PDA footprint, using indoor wideband channel measurements at 5.2 GHz alongside channel simulations. A channel model which employs the plane-wave approximation was used to combine the embedded antenna radiation patterns of the candidate devices obtained from far-field pattern measurements and multipath component parameters from an indoor ray-tracer. The 4-element candidate arrays were each constructed using a different type of antenna element, and despite the diverse element directivities, pattern characteristics, and polarization purities, all three devices were constructed to fully exploit diversity in polarization, space, and angle. Thus, low correlation and high information theoretic capacity was observed in each case. A good match between the model and the measurements is also demonstrated, especially for 2×2 MIMO subsets of identically or orthogonally polarized linear slot antennas. The interdependencies between the channel XPD, directional spread and pathloss, and the respective impact on channel capacity are also discussed in this paper.

Copyright © 2007 Arindam Pal et al. This is an open access article distributed under the Creative Commons Attribution License, which permits unrestricted use, distribution, and reproduction in any medium, provided the original work is properly cited.

1. INTRODUCTION

Multiple-input multiple-output (MIMO) wireless systems employing multielement arrays (MEAs) at both ends of a wireless link can in principle offer significantly greater spectral efficiencies than those available through conventional single antenna systems [1]. Enhanced data-throughput is achieved by either combining received signals to achieve diversity gain [2], or by establishing parallel subchannels if the correlation between fading of the transmitter-receiver (Tx-Rx) pairs is sufficiently low [3]. Correlation in a MIMO channel is governed by the characteristics of the radio channel, as well as the response of the array elements. The provision for multiple antennas on portable devices, such as laptops, PDAs (personal digital assistant) and mobile phones, presents numerous design challenges in terms of the choice and placement of antenna elements within the limited space available. These design choices influence the diversity gain that can be achieved from the spatial, polarization, and directional domains [4], and ultimately the performance of the communication system. Antenna selection schemes, mutual coupling, and power allocation strategies are some of the

additional design aspects which should also be considered [5]. Several cost- and space-efficient antenna designs have been proposed, which include use of cross-dipoles or dual-polarized patch antennas for polarization diversity [6, 7] or space-polarization diversity [8] and planar inverted-F antennas (PIFA) for space-pattern diversity [9].

In order to make an accurate evaluation or comparison of any proposed array designs, channel measurements in a large number of propagation environments are ideally needed to determine the overall channel and antenna response. However, extensive measurement trials are not easily realizable. Moreover, direct channel measurements offer limited scope for a comprehensive analysis of the channel and antenna facets since the data is often limited and generally cannot be separated into propagation only and antenna only domains. (Double directional channel measurements can provide channel only responses [10–12], however these can have a restricted view of the channel as full 3D characterization in both space and polarization is difficult to achieve.) In addition, measured channels will not indicate how the scatterers in the environment or the imperfect polarization responses of the antennas each impact

the combined antenna and channel polarization response. Therefore, computer-based models employing rigorous analysis of both the channel and the antennas are needed in addition to direct measurements, in order to facilitate accurate and rapid evaluations of proposed antenna designs.

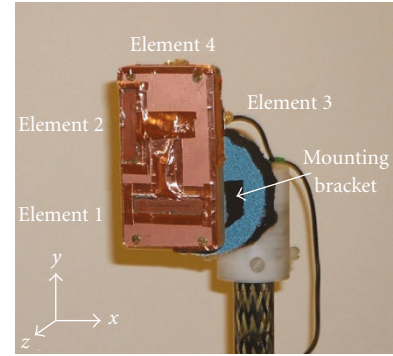
In this paper, an evaluation of three candidate antenna array designs embedded in PDA-type devices is presented using channel measurements as well as channel modeling. Wideband MIMO channel measurements between pairs of identical candidate devices were conducted in an open-plan office environment at a centre frequency of 5.2 GHz. The candidate arrays also were directly measured for their three-dimensional (3D) radiation patterns in a certified anechoic chamber. A validated ray-tracing model of the environment chosen for the channel measurements was used to extract the spatio-temporal parameters of multipath components propagating between the transmitting and receiving points. A channel model that combines this information was used to predict the inclusive MIMO antenna and channel response. The model relies on the plane-wave assumption as the antenna patterns and the multipath gains are resolved in two orthogonal polarizations that are also orthogonal to the direction of propagation. The 4-element candidate arrays were each constructed using a different type of antenna element. These elements offer widely different radiation pattern characteristics, efficiencies, polarization purities, and directivities. The elements were placed on each device with the aim to exploit the diversity in polarization, space, and angle, hence providing low-pattern correlation and high-channel capacities. A good match was found between the model and the measurements in terms of the information theoretic capacity, especially for 2×2 MIMO subsets comprising of identically or orthogonally polarized linear slot antennas. The interdependencies between channel cross-polar discrimination (XPD), directional spread and pathloss, and the associated impact on MIMO capacity are also discussed in this paper.

2. CANDIDATE ANTENNA ARRAYS

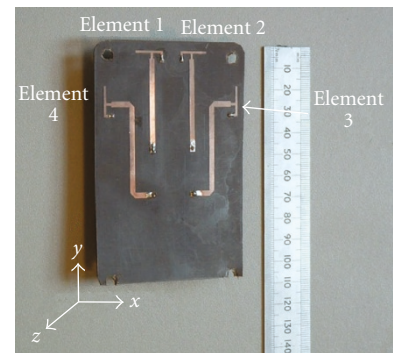
2.1. Construction of candidate arrays

The three 4-element designs use the same type of element throughout and were designed to mount on the surface of a PDA-type case of dimensions $63 \times 113 \times 14$ mm. The element placements within the devices can be seen in Figure 1. The three element types evaluated here were cavity backed linear slots (slot), planar inverted-F (PIFA), and the dielectric resonator antenna (DRA). All the elements were designed to operate at 5.2 GHz, with a -10 dB input reflection coefficient bandwidth in excess of 120 MHz.

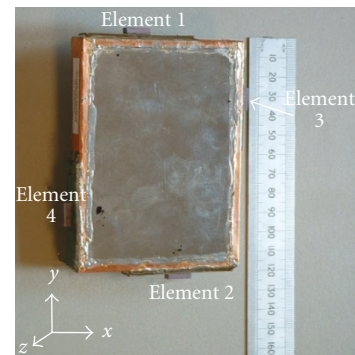
The slot antenna was fabricated using 1.6 mm thick Rogers RT/duroid 5880, with an individual element measuring $40 \times 14 \times 3.2$ mm. Four slots were flush-mounted on a suitable diecast box, see Figure 1(a), with element 1 located on the front of the PDA in the position between the function buttons and the screen. Element 2 was located on the front of the PDA to the left of the screen position. Element 3 was located on the right-hand side at the top of the



(a) Slot



(b) PIFA



(c) DRA

FIGURE 1: Candidate 4-element PDA-type devices.

case, and Element 4 was located centrally on the top edge of the case. The PIFAs were fabricated on 0.8 mm Taconic TLY5 with a dielectric constant of 2.2. The radiating surface covered 13.5×3.5 mm beyond the ground plane and 4 such elements were mounted approximately 21 mm apart within the PDA and placed towards one end of the device such that when the PDA is held in the hand, the antennas are well removed from the normal hand position as shown in Figure 1(b). The DRA-based design employed a ceramic puck measuring $11 \times 4.8 \times 3.2$ mm mounted on a small PCB assembly of 50×10 mm. Four single elements were soldered

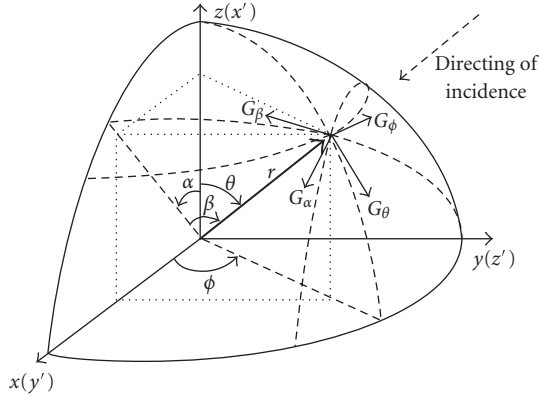


FIGURE 2: Directions of polarization components in (θ, ϕ) and (α, β) spherical coordinate systems.

to a PDA sized copper box, located one on each edge of the box as shown in Figure 1(c). The elements were placed with the aim to maximise pattern coverage, while directing energy away from the circuit board of the device and the other elements in order to minimise electromagnetic interference (EMI) and maximise antenna to antenna isolation, respectively. The placement of elements in each device was chosen to provide diversity in polarization, beam-angle, and space, in order to facilitate stable average signal-to-noise ratio (SNR) and low correlation.

2.2. Measured antenna patterns

The far-field 3D complex radiation patterns of the three candidate antenna arrays (mounted on a PDA-type case) were measured at 5.2 GHz in an anechoic chamber at the University of Bristol, using a system of measurement similar to that described in [13]. The measurement process involves rotation of the antenna-under-test (AUT) with respect to a fixed reference antenna placed in the far-field region (to allow plane-wave assumption). In order to include the effect of the casing and the adjacent elements on the radiation patterns of each element, the entire PDA-type devices containing the arrays were used as AUTs. The phase patterns for all elements were referenced to a point on the device rather than the element phase center, and therefore include all the phase information relevant for MIMO simulations. In addition, the effects of mutual coupling were also included in the measured patterns since all of the elements were present and every unused port terminated in 50 ohms. The 3D element radiation patterns were measured at uniform separations of the angles θ and ϕ (see Figure 2). In each direction (θ, ϕ) , the amplitudes and phases were measured in two orthogonal polarization planes, which are also orthogonal to the direction of the incoming electric field. The antenna gain in a given direction of radiation (θ, ϕ) is represented by the vector $\mathbf{g} = [G_\theta(\theta, \phi)G_\phi(\theta, \phi)]$, where $G_\theta(\theta, \phi)$ and $G_\phi(\theta, \phi)$ are the dimensionless complex gains that are parallel to the directions of rotation of θ and ϕ , respectively.

TABLE 1: Antenna element properties of the three types of antennas.

Antenna	Directivity	Efficiency	Copolar power	Antenna XPD
Slot	7.8 dBi	81.4% \pm 3.7%	94%	12.2 dB
DRA	4.6 dBi	39.0% \pm 2.7%	81%	4.8 dB
PIFA	5.8 dBi	60% \pm 5%	59%	N/A ⁽²⁾

⁽²⁾ XPD is not defined for the PIFA since the primary polarization mode cannot be defined for this structure.

2.3. Candidate antenna properties

A summary of the directivities, radiation efficiencies, and copolar powers derived from the pattern measurements is shown in Table 1. Here, the copolar power, also referred to as ‘‘polarization purity,’’ is the percentage of radiated power that can be resolved to a single polarization plane. The antenna XPD was obtained as the ratio of maximum copolar power to maximum cross-polar power. The directivity is given by ratio of the power radiated in the direction of maximum gain to the total radiated power. The overall radiation efficiency, as given by the ratio of overall radiated power to the power applied to the input terminals of an antenna, was estimated using the procedure described in [14].

From Table 1, it can be seen that the slot antenna offers the highest efficiency and directivity as well as the greatest polarization purity. The DRA offers moderate polarization purity, but has a lower efficiency, whereas the PIFA has slightly better efficiency when the total radiated power is considered, but very little cross-polar discrimination.

3. CHANNEL MODEL

An account of the multipath parameters obtained from the site-specific model is given in Section 3.1. The post-processing of the measured antenna radiation patterns in order to match them with the measurement setup is detailed in Section 3.2. The channel model that calculates the inclusive MIMO antenna and channel response using the polarization-resolved antenna patterns and complex multipath component gains is explained in Section 3.3.

3.1. Deterministic channel characterization

The radio propagation characteristics of an open-plan office of dimensions $12 \times 18 \times 8$ m was simulated using the ray-launching algorithm [15]. The model accounts for diffraction of multipath waves. However, like most deterministic models, diffuse scattering components (from rough surfaces) are not considered. The extracted multipath components gains were resolved in 3D directions as well as orthogonal polarizations at the transmitter and receiver ends. The 3D modeling is critical as the devices are likely to operate in indoor environments where scattering in the elevation domain is significant. The multipath parameters were derived for a transmitter placed at a central location in the room (close to Rx-1 in Figure 4) and multiple receiver deployments placed at about 4000 evenly spaced points throughout the area. The

TABLE 2: Correlation coefficients between directional spread, channel XPD, Pathloss, and K-factor, calculated using multipath component parameters extracted from ray tracing.

Channel properties	σ_Ω DOD	σ_Ω DOA	XPD dB	Pathloss dB	K-factor dB
σ_Ω DOD	1.00	—	—	—	—
σ_Ω DOA	0.45	1.00	—	—	—
XPD dB	-0.70	-0.60	1.00	—	—
Pathloss dB	0.65	0.49	-0.74	1.00	—
K-factor dB	-0.35	-0.25	0.50	-0.44	1.00

heights of the transmitter and the receiver were chosen to match those used in the measurements (Section 4). The extracted multipath rays at each Tx-Rx location were described by their DOAs, DODs, excess delays, gains and phases. The multipath gains were obtained for the four combinations of Tx-Rx polarizations, as given by $h_{\theta\theta}$, $h_{\phi\phi}$, $h_{\theta\phi}$, and $h_{\phi\theta}$.

The average MIMO capacity for any antenna array design is dependent on the statistics of a number of channel parameters, which include the directional spread, channel XPD, pathloss, and K-factor. These channel parameters were calculated using the extracted multipath component parameters. The channel XPD is defined as the ratio of power transferred within the same polarization to the power coupled to the orthogonal polarization, and was calculated using (1),

$$\text{XPD} = \frac{\sum_{s=1}^S |h_{\theta\theta,s}|^2 + |h_{\phi\phi,s}|^2}{\sum_{s=1}^S |h_{\theta\phi,s}|^2 + |h_{\phi\theta,s}|^2}. \quad (1)$$

The channel XPD was found to be in the range of -5 to 25 dB over all locations of the receiver in the ray-tracing model. The directional spread of the multipath energy distribution was calculated using the “tr[**R**]” metric proposed in [16], and will be denoted here as σ_Ω . The RMS delay spreads were found to be largely in the range of 5 to 10 nanoseconds. The K-factor was estimated as the ratio of power in the fixed dominant component (maximum power path) to the total power in the other paths. The variation of these channel parameters with the locations of the transmitter and the receiver is not mutually independent. A summary of correlation coefficients (calculated using significance level of 95%) between these parameters, calculated over all ray-traced locations, is given in Table 2.

3.2. Post-processing of measured antenna patterns

The same (θ, ϕ) coordinate system was used to define the directions and polarization components of the multipath components as well as the antenna radiation patterns. However, the device orientation for which the measured antenna patterns were defined did not correspond to that used in the channel measurements. The following transformation was therefore applied to the measured antenna radiation patterns before embedding them in the channel simulations.

The measured radiation patterns are such that an azimuth rotation of the candidate devices in the channel mea-

surements corresponds to a rotation in the $\phi = 0$ or x - z plane in the measured antenna patterns (Figure 2). The plane perpendicular to the x - z plane that contains the direction of incidence \mathbf{r} corresponds to the elevation plane. Therefore, the aim is to calculate the gain components G_α and G_β , which are perpendicular to \mathbf{r} and parallel to the directions of rotation of α and β , respectively. The angles α and β represent the azimuth and elevation angles, respectively. From Figure 2, it can be observed that (α, β) and (θ, ϕ) follow a similar spherical coordinate system with respect to the (x', y', z') and (x, y, z) Cartesian coordinate systems, respectively. For any α and β , θ and ϕ can be calculated using (2), respectively,

$$\begin{aligned} \theta &= \arccos(\cos \beta \cos \alpha), \\ \phi &= \arctan\left(\frac{\tan \beta}{\sin \alpha}\right). \end{aligned} \quad (2)$$

The repolarization is achieved by first expressing the original measured pattern gains (G_θ, G_ϕ) as Cartesian components (G_x, G_y, G_z) , as shown in (3), and reconverting to spherical coordinate components (G_α, G_β) , as shown in (4),

$$\begin{bmatrix} G'_y \\ G'_z \\ G'_x \end{bmatrix} = \begin{bmatrix} G_x \\ G_y \\ G_z \end{bmatrix} = \begin{bmatrix} \sin \theta \cos \phi & \cos \theta \cos \phi & -\sin \phi \\ \sin \theta \sin \phi & \cos \theta \sin \phi & \cos \phi \\ \cos \theta & -\sin \theta & 0 \end{bmatrix} \begin{bmatrix} G_r \\ G_\theta \\ G_\phi \end{bmatrix}, \quad (3)$$

$$\begin{bmatrix} G_r \\ G_\beta \\ G_\alpha \end{bmatrix} = \begin{bmatrix} \cos \beta \cos \alpha & \cos \beta \sin \alpha & \sin \beta \\ \sin \beta \cos \alpha & \sin \beta \sin \alpha & -\cos \beta \\ -\sin \alpha & \cos \alpha & 0 \end{bmatrix} \begin{bmatrix} G_z \\ G_x \\ G_y \end{bmatrix}. \quad (4)$$

Note that G_r is the gain component parallel to \mathbf{r} , and should be equal to zero. As a check, (5) must hold true for any direction, since the absolute gain is preserved,

$$|G_\beta(\alpha, \beta)|^2 + |G_\alpha(\alpha, \beta)|^2 = |G_\theta(\theta, \phi)|^2 + |G_\phi(\theta, \phi)|^2. \quad (5)$$

The re-resolved antenna gain patterns (G_α, G_β) were applied in the channel model described in Section 3.3. However, the (G_θ, G_ϕ) notation will be used in the remaining part of the paper.

3.3. MIMO channel model with polarization

The electromagnetic wave impinging upon an antenna is a space-varying vector quantity that can be resolved into 3 orthogonal spatial vector components, and has three distinguishable electric states of polarization at a given point [17]. The measured antenna patterns and extracted multipath component gains implicitly use the plane wave assumption, which dictates that the electric field is resolvable into two orthogonal polarizations that are also orthogonal to the direction of propagation. The inclusive antenna and channel gain $H_{m,n,l}$ from transmit element n to receive element m at

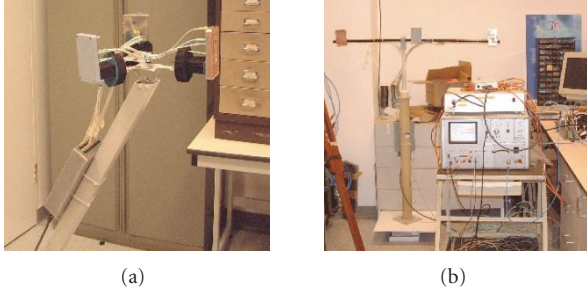


FIGURE 3: Channel measurement setup. (a) Receiving station; (b) transmitting station.

the l th delay tap of the wideband channel is given by

$$H_{m,n,l} = \sum_{s=1}^{S_l} (\mathbf{g}_{T,n}(\Omega_{T,s}))^T \begin{bmatrix} h_{\theta\theta,s} & h_{\theta\phi,s} \\ h_{\phi\theta,s} & h_{\phi\phi,s} \end{bmatrix} \mathbf{g}_{R,m}(\Omega_{R,s}), \quad (6)$$

where S_l is the number of rays at the l th delay tap. The subscript l has been omitted in the remaining part of (6) for clarity. Since a ray-tracer provides path delays with infinite resolution, an arbitrary tap separation can be chosen and all the paths can be resolved to the nearest tap. Here, 97 taps at a separation of 8.33 nanoseconds were used, so as to match the measurement settings (97 frequency fingers over bandwidth of 120 MHz). In (6), $\Omega_{T,s}$ and $\Omega_{R,s}$ are the direction of departure (DOD) and direction of arrival (DOA) of the s th multipath ray, and $\mathbf{g}_{T,n}$ and $\mathbf{g}_{R,m}$ are the antenna gain vectors at the n th transmitter and m th receiver, respectively. Note that in (6), the directions of polarization components match at each antenna-channel interface. For instance, $h_{\theta\phi}$ is multiplied by the G_θ component at the transmitter and the G_ϕ component at the receiver. The effects of mutual coupling and the phase differences caused by spatial separation of the elements are included within the complex antenna radiation patterns, as explained in Section 2.2.

4. MIMO CHANNEL MEASUREMENTS

Wideband MIMO channel measurements were conducted using the three candidate devices with the aim to determine which design offered the best performance in terms of information theoretic capacity. The measurements were conducted simultaneously for all 3 PDA-type candidate devices using a Medav RUSK sounder operating in a peer-to-peer communications scenario [18]. The transmitting devices were arranged on a horizontal boom at 1.3 m above the floor with approximately 0.75 m between the devices (Figure 3). At the receiving station the 3 devices were placed on a short triangular arm, and the centre of this structure mounted on a rotating arm putting the devices at 1.3 m above the floor whilst transcribing a circular path of radius 0.5 m. The circular motion was employed to avoid static nulls in the data relating to a particular location. Using this setup of 3 pairs of candidate arrays, all constituent subchannel links were measured in succession at every position of the rotat-

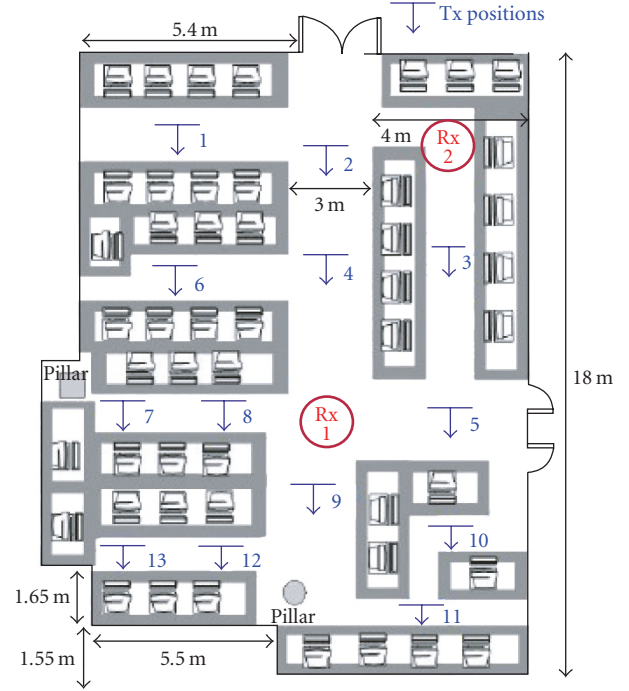


FIGURE 4: Open-plan office used for deterministic modeling and channel measurements.

ing arm. During each full rotation (360°) of the rotating arm, which took approximately 10 seconds to complete, 1000 MIMO recordings were taken. These recordings were made for several locations of the transmitting station around the room, while the receiving station was fixed at a central location. See Figure 4 for the floor plans noting that the arrow refers to the broadside direction of the array mounting boom.

The transmitter employed a periodic multitone signal with a bandwidth of 120 MHz, centered on 5.2 GHz and a multitone repetition period of $0.8 \mu\text{s}$. Equal power was applied to each transmit antenna. Further details of the measurement campaign can be found in [18].

5. CALCULATION OF CAPACITY

Since power was allocated equally to each transmit element and frequency carrier, and the carriers were equally spaced in frequency, the information theoretic capacity averaged over the entire bandwidth was calculated using (7) [1],

$$C = \frac{1}{n_f} \sum_{f=1}^{n_f} \log_2 \left(\det \left(\mathbf{I}_M + \frac{\rho}{N} \mathbf{H}_f \mathbf{H}_f^* \right) \right) \text{ bits s}^{-1} \text{ Hz}^{-1}, \quad (7)$$

where \mathbf{H}_f is the $M \times N$ dimensional channel response matrix at frequency component f , M and N are the numbers of receive and transmit elements, n_f is the number of frequency carriers, $*$ is the complex conjugate, and ρ is the average SNR at each receiver branch over the entire bandwidth. Note that

\mathbf{H}_f usually represents a power normalized channel response, and the capacity is calculated using a fixed chosen SNR. Normalization is required primarily to make the analysis independent of large scale channel fading statistics. The following section will discuss two types of channel normalization, gain- and pathloss-normalization, both of which will be applied to the channel model and the channel measurements.

5.1. MIMO channel gain normalization

Since capacity is a function of the received SNR, which varies with the location of the transmitting and receiving antennas, the normalized channel response (\mathbf{H}) is commonly derived from the observed response (\mathbf{T}) to give average received power of unity, as given by [9]. Here, both \mathbf{T} and \mathbf{H} have dimensions of $M \times N \times n_f$,

$$\mathbf{H} = \frac{\mathbf{T}}{\sqrt{1/(M \times N \times n_f) \sum_{f=1}^{n_f} \sum_{m=1}^M \sum_{n=1}^N |\mathbf{T}_{m,n,f}|^2}}. \quad (8)$$

The above normalization entirely compensates for the total received power in a MIMO channel snapshot and will be referred to as gain normalization. The gain-normalized capacity is related to the rank of the channel and gives a measure of the correlation between the antennas.

5.2. Channel pathloss normalization

For any given location of the transmitter and the receiver, the average received power varies between antenna array designs, as it is influenced by the element beamwidths, element orientation, device orientation as well as radiation efficiency. Since the focus of this analysis is a comparison between candidate array designs, as opposed to the locations of measurement, an estimate of capacity that also accounts for the relative received powers by the various devices is required. The proposed solution is to compensate the channel response only for the large-scale fading component or the average propagation pathloss between the transmitting and receiving locations. Unlike gain normalization, the same pathloss normalization factor is used for all the devices. Note that equal transmit power was used for each device. The pathloss normalization is given by (9)

$$\mathbf{H} = \mathbf{T} \cdot \sqrt{\eta \cdot n_f / P_T}, \quad (9)$$

where η is the pathloss and P_T is the power radiated by each transmitting element. η is given by the ratio between the transmitted and the received power using ideal isotropic radiators at the terminals. The average channel gain of the pathloss normalized channel response can be expected to be unity for ideal isotropic radiators. The pathloss normalized capacity accounts for channel rank as well as the power losses at the antenna terminals.

5.3. Pathloss normalization for the model

For a unipolar link, the pathloss is given by

$$\eta = \frac{1}{\sum_{s=1}^S |h_s|^2}, \quad (10)$$

where h_s is the complex gain of each multipath wave. However, the candidate arrays radiate different levels of powers in the horizontal and vertical polarization planes, and the unequal pathloss in the orthogonal polarizations must be accounted for. Therefore, a summation of multipath power gains weighted by the ratio of power transmitted in that polarization was used in the estimation of pathloss, as given by

$$\eta = \frac{P_T n_f}{r_\phi \sum_{s=1}^S (|h_{\phi\theta,s}|^2 + |h_{\phi\phi,s}|^2) + r_\theta \sum_{s=1}^S (|h_{\theta\phi,s}|^2 + |h_{\theta\theta,s}|^2)}, \quad (11)$$

where r_ϕ and r_θ are the ratios of power transmitted in the horizontal (ϕ) and vertical (θ) polarizations, respectively, as given by (12). Note that ($r_\phi = 1 - r_\theta$),

$$r_\phi = \frac{\sum_{n=1}^N \int_0^{2\pi} \int_0^\pi |G_h(\theta, \phi)_n|^2 \sin \theta d\phi d\theta}{\sum_{n=1}^N \int_0^{2\pi} \int_0^\pi (|G_v(\theta, \phi)_n|^2 + |G_h(\theta, \phi)_n|^2) \sin \theta d\phi d\theta}. \quad (12)$$

The estimates of channel pathloss given by (11) were applied in (9) to normalize the model-based MIMO channel responses.

5.4. Pathloss normalization for the measurements

Unlike the ray-tracer-based model, the channel measurements did not provide a direct estimate of the omni-directional pathloss as the candidate antennas were neither sufficiently isotropic in pattern, nor placed to provide perfectly uniform directional coverage. Pathloss increases with the distance between the transmitting and receiving stations, but also depends on the objects in the environment which can block a direct path between the two ends. Therefore, the only available method for estimating pathloss in the measured channels is to consider a difference (in dB) between the transmitted power and the measured received powers. Due to the directivity of the antenna element patterns as well as spatial fading effects, at any given location and orientation of the arrays, some of the Tx-Rx element pairs are likely to be illuminated while others might be shadowed. An average of the received power over all transmitting and receiving elements would result in an over-estimation of pathloss due to the inclusion of the shadowed Tx-Rx links. Therefore, pathloss normalization factor for each measurement location was assigned to be equal to the mean of the highest 1% of all constituent SISO subchannel power gains from all candidate arrays. These approximate estimates were confirmed to be within a similar range as those derived from the model.

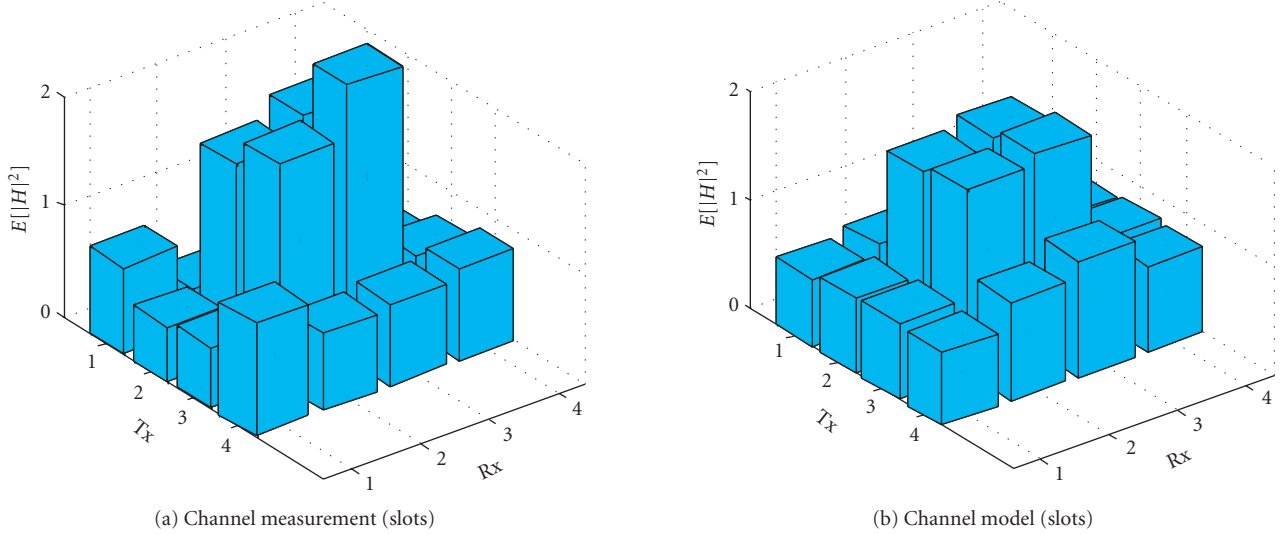


FIGURE 5: Average powers of normalized 4×4 MIMO channel responses for the slot antenna devices, obtained from (a) channel measurement and (b) channel model.

The same channel pathloss estimates were used for the three candidate arrays.

6. MIMO CAPACITY ANALYSIS

The calculation of pathloss-normalized capacity employs estimates of antenna efficiencies and the channel pathloss, which are difficult to determine accurately for real antennas and channel measurements. Due to the separation of the 3 PDA arrays on the Tx mounting assembly, the Tx-Rx distances and hence the pathlosses of the three PDA links were significantly different when the receiving station was placed close to the transmitters. Since the same pathloss normalization factor was used for the three candidate arrays, only measurement locations that had relatively large Tx-Rx separations were used for comparison with the model. Tx locations 4, 5, 8, 9, and 10 were excluded because of their proximity to Rx 1 (see Figure 4). A comprehensive validation of the model would require determining the antenna locations and orientations that were used for the channel measurements. Such a validation was not attempted, mainly because the ray-tracing model does not account for all the geometrical and material complexities of the actual environment. Objects that lead to additional scattering but are not accounted for in the model include the furniture and equipment in the room. Therefore, the combined capacity over all locations (about 4000) of the receiver in the ray-tracing model has been compared with that of the chosen measurement locations. Thus, a very close match between the model and the measurements is not expected.

6.1. Received power

Antenna diversity, such as the polarization diversity in the slot devices, can lead to substantial power imbalances. The

mean power gains of the normalized MIMO channel matrices, calculated over all chosen locations from the model and the measurements, are shown for the slot devices in Figure 5. Elements 2 and 3 in the slot array radiated predominantly in the azimuth plane in horizontal polarization, whereas the elements 1 and 4 radiated vertically polarized waves in a given elevation plane. Since the movements of the transmitter and receiver devices were confined within the azimuth plane, the slot elements 2 and 3 in the receiver arrays remained within the sector of radiation of the same elements in the transmitter. In contrast, subchannels linking elements 1 and 4 in the transmitter and receiver arrays are subject to both pattern and polarization mismatch for most orientations of the devices in the azimuth. Both the model and the measurements show that slot elements 2 and 3 provide on average the highest power 2×2 MIMO subset (Figure 5). The match between the model and the measurements validates the repolarization procedure that was applied to the measured antenna patterns (Section 3.2).

The distribution of average received power over the constituent subchannels of the DRA- and PIFA-based MIMO channels was found to be more uniform than that of the slots (Figure 6). This can be attributed to the relatively lower directivities and polarization purities of the DRA and PIFA elements, which result in less antenna pattern mismatches.

6.2. 2×2 MIMO copolarized and cross-polarized facets

A requirement of the model is to provide a qualitatively correct comparison of performance of the candidate antenna designs, in particular the comparison of different antenna polarization schemes. The slot and the DRA arrays both comprise several pairs of either copolarized or cross-polarized (or orthogonally polarized) elements. A cross-polarized and a copolarized subset of the slot device were

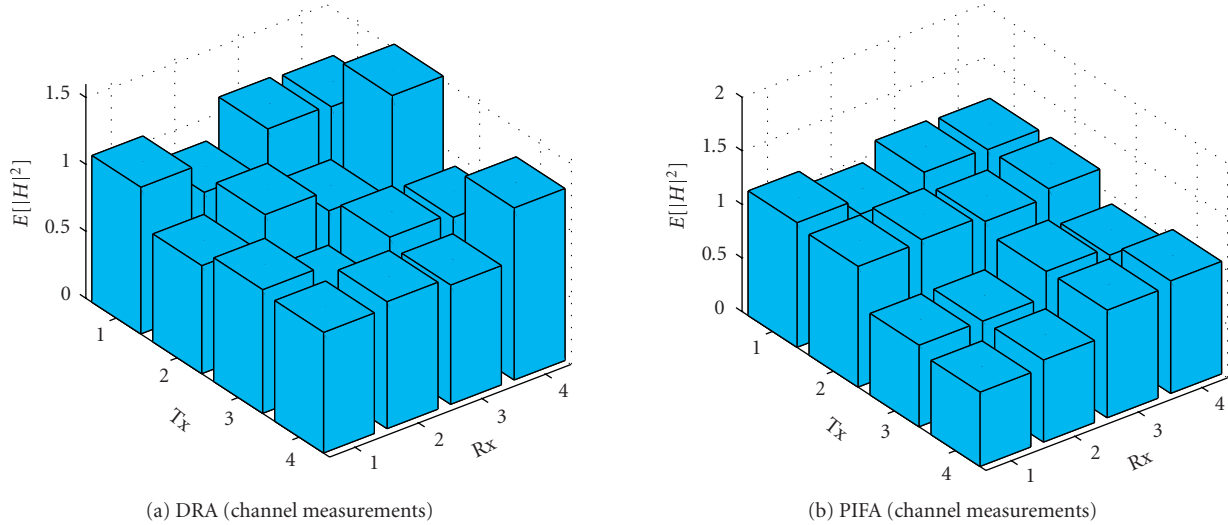


FIGURE 6: Average powers of normalized 4×4 MIMO channel responses, as obtained from the channel measurements for the (a) DRA and (b) PIFA arrays.

chosen for the analysis, the former comprising elements 1 and 2, and the latter comprising elements 2 and 3, as labeled in Figure 1(a). The slot device was chosen for this analysis instead of the DRA because slot elements have higher polarization purity. Note here that the copolar slots (elements 2, 3) radiate in opposite directions, whereas the cross-polar slots (elements 1, 2) radiate in the same direction. Thus, the copolar subset provides a better directional pattern diversity in the azimuth plane.

The model and the measurements both confirm that the cross-polarized slots achieve better decorrelation than the copolarized slots, as shown in Figure 7. The underestimation of gain-normalized capacity by the model in relation to the measurements was anticipated from the observations reported in [19], as low power or diffuse components were not extracted by the model. The model underestimates the median capacity of the copolar slots' channel by 0.35 bits/s/Hz and that of the cross-polar slots' channel by 0.37 bits/s/Hz. Thus, the level of underestimation of gain-normalization is very similar for the two 2×2 MIMO subsets.

As explained in Section 6.1, the orientations of the transmitting and receiving devices were such that the antenna pattern mismatch in the copolarized subset was minimal. In addition, the copolar elements exploited the directional diversity in the azimuth to a greater extent than the cross-polar elements. Hence, the copolar channel received high and stable total powers over all locations. When compared with the cross-polar subset, the higher power received by the copolar array compensated for its higher correlation, leading to better pathloss-normalized capacity, as shown by both the model and the measurements (Figure 8). The differences between the median pathloss-normalized capacities given by the model and the measurements are 1.1 bits/s/Hz for the cross-polar slots and 0.5 bits/s/Hz for the copolar slots. These discrepancies are marginally greater than that of the gain-

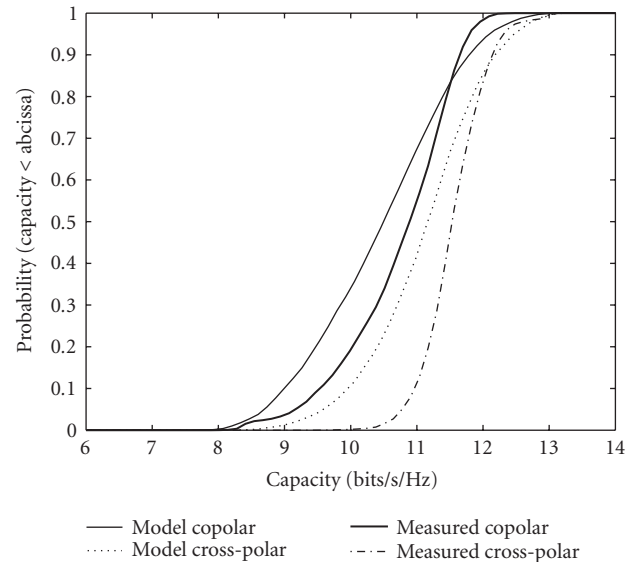


FIGURE 7: Gain-normalized capacities of 2×2 MIMO copolarized and cross-polarized subsets of the slot devices, calculated for $\text{SNR} = 20$ dB.

normalized capacities due to inaccuracies in estimation of the channel pathloss distributions (especially the measured channels).

For further interpretation of the channel capacity results, the effect of channel properties must be taken into account. The channel XPD is high in the presence of a strong LOS component and decreases as multipath scattering increases, as can be seen from Table 2 or [20, 21]. Rich directional scattering reduces the channel XPD and leads to poorer isolation between the orthogonal streams of the dual-polarized

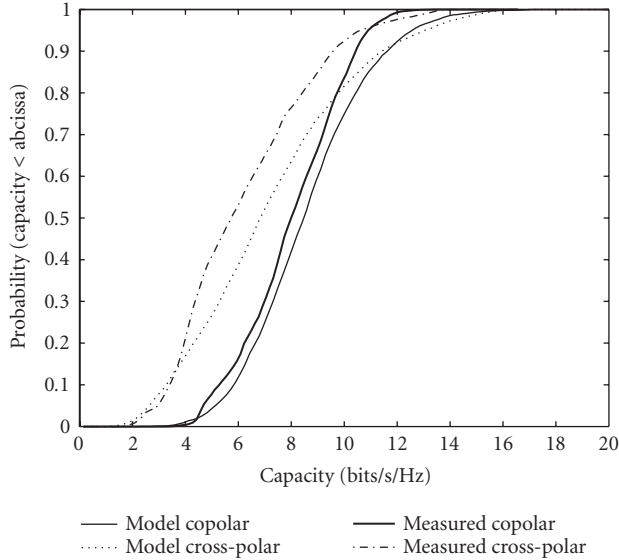


FIGURE 8: Pathloss normalized capacities of 2×2 MIMO copolarized and cross-polarized subsets of the slot devices, calculated for SNR = 20 dB.

channel. It has been shown experimentally that the advantage of dual-polarized antennas over single polarization antennas improves at short ranges in LOS conditions, as the higher rank (due to high channel XPD) compensates for the channel XPD-based power losses [22]. These dependencies between K-factor, directional spread, and channel XPD present a trade-off that could be exploited by a combination of space- and polarization-diversity antennas-parallel sub-channels can be established through polarization diversity in high channel XPD (or LOS) conditions where spatial diversity is likely to be poor, and the space diversity aspect of the antennas provide the decorrelation in locations with rich directional scattering (poor channel XPD). This arrangement of antennas is employed by the cross-polarized subset of the slot PDA. The negative correlation between the channel XPD and directional spread (Table 2) compensates for their positive effects on the channel rank of the cross-polarized slots' MIMO channel. Hence, the gain-normalized capacities obtained from the cross-polarized arrays show lower overall variation over all considered locations (Figure 7), as well as lower dependency on channel parameters (Table 3), than that of the copolarized channel.

The random orientation or rotation of the transmitter and receiver devices in the 3D space is an important consideration for arrays with high-element XPDs. Although superior capacities can be achieved by copolarized antenna arrays (Figure 8), these links would fail if the transmitter and receiver become mismatched in polarization due to device rotation [23]. However, the construction of the slot device is such that when the device is tilted by 90° , so that the long side of the PDA is horizontal, elements 1 and 4 effectively replace elements 2 and 3, radiating horizontally polarized waves omnidirectionally in the azimuth. Thus, a simple antenna selection scheme that selects the 2×2 MIMO subset receiving the

TABLE 3: Correlation coefficients between gain-normalized capacity of the slots' copolar and cross-polar 2×2 MIMO channels and the channel parameters. σ_Ω denotes the 3D directional spread of multipath energy distribution.

Channel properties	Gain-normalized capacity bits/s/Hz	
	Cross-polar slots elements (1, 2)	Copolar slot elements (2, 3)
σ_Ω DOD	-0.03	0.23
σ_Ω DOA	0.001	0.18
Channel XPD dB	0.05	-0.23
Pathloss dB	-0.10	0.21
K-factor dB	0.004	-0.23

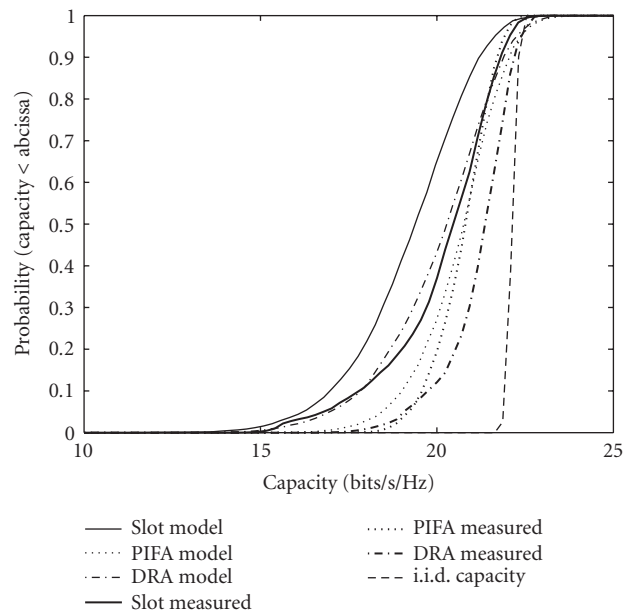


FIGURE 9: Gain-normalized capacities of the 4×4 MIMO links, from simulations and measurements, calculated for SNR = 20 dB.

highest power can potentially provide consistent 2×2 MIMO system performance.

6.3. 4×4 MIMO channels

The differences between the gain-normalized capacities of the various 2×2 subsets of the DRA and PIFA devices were negligible. This can be inferred from the high 4×4 MIMO gain-normalized capacities of these devices (close to i.i.d. capacity, as shown in Figure 9), which implies that their constituent 2×2 MIMO subsets must also be highly decorrelated. The result also indicates that the polarization diversity in the DRA device was not as evident as the slot device, which could be due to the limited XPD of the DRAs [24]. Low correlation between all the DRA elements was achieved from good isolation in space and angle instead. The low XPD and directivities of the PIFAs and DRAs lead to less polarization mismatch and pattern mismatch, respectively. This can also be expected

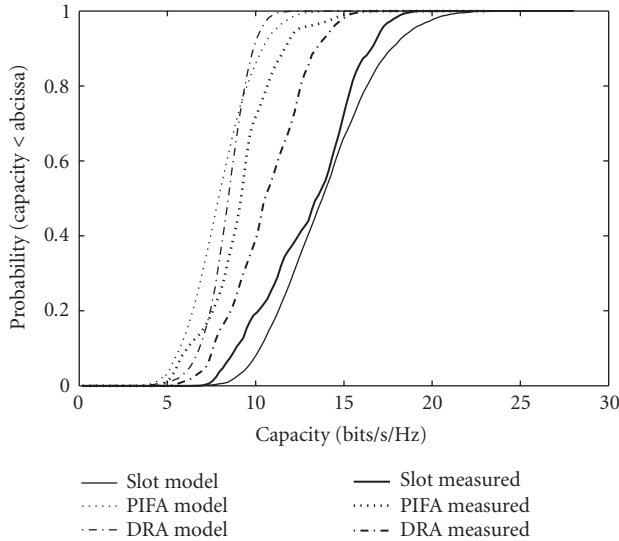


FIGURE 10: Pathloss normalized capacities of the 4×4 MIMO links, from simulations and measurements, calculated for SNR = 20 dB.

to lower power imbalances and aid diversity gain. The lower likelihood of polarization or pattern mismatch would also lend stability to performance if the devices are rotated arbitrarily.

The high gain-normalized capacities of the 4×4 MIMO channels can be attributed to the antenna diversity in polarization, space and angle in the devices, as well as rich scattering in the channel. Both the model and the measurements show that the slots devices achieve the lowest gain-normalized capacity. This is explained by the relatively higher correlation of its copolarized elements. The relatively high antenna efficiency of the slot devices aid them to receive more power and achieve the best pathloss normalized capacities, as shown in Figure 10. The performance of the PIFAs was affected by the outer case containing the antennas, contributing to further attenuation by about 1 dB at each end. The pathloss-normalized capacity of the DRA devices was affected by their relatively low radiation efficiency. The differences in the pathloss normalized capacities between the model and the measurements are due to either inaccurate estimation of antenna efficiency and pathloss, or inaccuracy in multipath component characterization in the model. The DRAs, for instance, have low directivities and rely on directional scattering, so the absence of significant directional paths in the ray-model would lead to an underestimation of their gain- and pathloss-normalized capacity.

7. CONCLUSIONS

An evaluation of three 4-element candidate array designs, embedded in PDA-type devices and operating in MIMO peer-to-peer schemes in an indoor environment, has been presented using channel measurement as well as channel modeling. The analysis shows a comparison of the information theoretic MIMO capacity between the antenna designs.

The channel capacity was calculated for two types of normalization: the gain-normalized capacity accounts for only the correlation in the channel, whereas the pathloss-normalized capacity also accounts for the powers received by the antennas. The latter calculation of capacity is more relevant if there is a constraint on the transmit power available. A good match between the model and measurements was demonstrated using 2×2 MIMO subsets of copolarized and cross-polarized slot elements. While the cross-polarized subset offers better decorrelation or isolation between its subchannels, the copolarized scheme achieves better overall performance due to higher received power. The placement of these linearly polarized elements in a combination of spatial and polarization diversity is particularly useful for exploiting the trade-offs between directional spread and channel XPD, resulting in stable gain-normalized capacities as the devices traverse through LOS and NLOS propagation scenarios. Despite the imperfect XPD of the DRAs and the negligible XPD of the PIFAs, these devices achieve low channel correlation, which indicates good spatial or angular isolation between the elements. Low element directivities and XPDs lead to less pattern or polarization mismatch, thus resulting in lower power imbalances as the device is rotated. For fixed transmit power, the slot devices offer the best capacities. The lower correlation within the DRA and PIFA devices partially compensates for their relatively inferior radiation efficiencies in terms of the observed MIMO capacities.

ACKNOWLEDGMENTS

The first author would like to thank the UK ORS scheme and the University of Bristol for his postgraduate scholarship. The authors would like to thank the UK Spectrum Regulator (Ofcom) for supporting the measurement campaign, as well as Chor Min Tan and Mythri Hunukumbure for their contributions during the trial programme. We are also grateful to University of York and Antenna for providing the PIFA and DRA multiantenna element PDAs. We would like to thank Beng Sin Lee and Prof. Andy Nix for their support in the use of the ray-tracing software, and Phill Rogers for his contribution to the development of the slot multielement PDA. The wireless measurement facilities and infrastructure provided through the Centre for Communications Research (CCR) at the University of Bristol are gratefully acknowledged.

REFERENCES

- [1] G. J. Foschini and M. J. Gans, "On limits of wireless communications in a fading environment when using multiple antennas," *Wireless Personal Communications*, vol. 6, no. 3, pp. 311–335, 1998.
- [2] R. G. Vaughan and J. B. Andersen, "Antenna diversity in mobile communications," *IEEE Transactions on Vehicular Technology*, vol. 36, no. 4, pp. 149–172, 1987.
- [3] D.-S. Shiu, G. J. Foschini, M. J. Gans, and J. M. Kahn, "Fading correlation and its effect on the capacity of multielement antenna systems," in *Proceedings of IEEE International Conference on Universal Personal Communications (ICUPC '98)*, vol. 1, pp. 429–433, Florence, Italy, October 1998.

- [4] C. B. Dietrich Jr., K. Dietze, J. R. Nealy, and W. L. Stutzman, "Spatial, polarization, and pattern diversity for wireless handheld terminals," *IEEE Transactions on Antennas and Propagation*, vol. 49, no. 9, pp. 1271–1281, 2001.
- [5] M. K. Özdemir, E. Arvas, and H. Arslan, "Dynamics of spatial correlation and implications on MIMO systems," *IEEE Communications Magazine*, vol. 42, no. 6, pp. S14–S19, 2004.
- [6] P. Kyritsi, D. C. Cox, R. A. Valenzuela, and P. W. Wolniansky, "Effect of antenna polarization on the capacity of a multiple element system in an indoor environment," *IEEE Journal on Selected Areas in Communications*, vol. 20, no. 6, pp. 1227–1239, 2002.
- [7] R. U. Nabar, H. Bölcskei, V. Erceg, D. Gesbert, and A. J. Paulraj, "Performance of multiantenna signaling techniques in the presence of polarization diversity," *IEEE Transactions on Signal Processing*, vol. 50, no. 10, pp. 2553–2562, 2002.
- [8] J. W. Wallace, M. A. Jensen, A. L. Swindlehurst, and B. D. Jeffs, "Experimental characterization of the MIMO wireless channel: data acquisition and analysis," *IEEE Transactions on Wireless Communications*, vol. 2, no. 2, pp. 335–343, 2003.
- [9] M. Karakoikis, C. Soras, G. Tsachtsiris, and V. Makios, "Compact dual-printed inverted-F antenna diversity systems for portable wireless devices," *IEEE Antennas and Wireless Propagation Letters*, vol. 3, no. 1, pp. 9–14, 2004.
- [10] B. H. Fleury, X. Yin, K. G. Rohbrandt, P. Jourdan, and A. Stucki, "High-resolution bidirection estimation based on the SAGE algorithm: experience gathered from field experiments," Tech. Rep. TD02(070), COST 273, Espoo, Finland, May 2002.
- [11] C. M. Tan, D. L. Paul, M. Beach, A. R. Nix, and C. J. Railton, "Dynamic double directional propagation channel analysis with dual circular arrays," in *Joint COST 273/284 Workshop on Antennas and Related System Aspects in Wireless Communications*, Gothenburg, Sweden, June 2004.
- [12] M. Landmann, A. Richter, and R. S. Thomä, "Estimation of multidimensional polarimetric channel model parameters," Tech. Rep. TD02(132), COST 273, Lisbon, Portugal, September 2002.
- [13] C. A. Balanis, *Antenna Theory, Analysis and Design*, Harper & Row, New York, NY, USA, 1982.
- [14] P. R. Urwin-Wright, G. Hilton, I. J. Craddock, and P. N. Fletcher, "A practical approach for reliably determining the efficiency of an antenna," in *Technical Seminar on Antenna Measurements and SAR*, pp. 27/1–27/4, Loughborough, UK, May 2002.
- [15] B. S. Lee, C. M. Tan, S. E. Foo, A. R. Nix, and J. P. McGeehan, "Site specific prediction and measurement of indoor power delay and power azimuth spectra at 5 GHz," in *Proceedings of the 54th IEEE Vehicular Technology Conference (VTC '01)*, vol. 2, pp. 733–737, Atlantic City, NJ, USA, October 2001.
- [16] A. Pal, M. Beach, and A. Nix, "A novel quantification of 3D directional spread from small-scale fading analysis," in *Proceedings of IEEE International Conference on Communications (ICC '06)*, vol. 4, pp. 1699–1704, Istanbul, Turkey, June 2006.
- [17] M. R. Andrews, P. P. Mitra, and R. deCarvalho, "Tripling the capacity of wireless communications using electromagnetic polarization," *Nature*, vol. 409, no. 6818, pp. 316–318, 2001.
- [18] M. Beach, M. Hunukumbure, C. Williams, et al., "An experimental evaluation of three candidate MIMO array designs for PDA devices," in *Joint COST 273/284 Workshop on Antennas and Related System Aspects in Wireless Communications*, Gothenburg, Sweden, June 2004.
- [19] A. F. Molisch, M. Steinbauer, M. Toeltsch, E. Bonek, and R. S. Thomä, "Capacity of MIMO systems based on measured wireless channels," *IEEE Journal on Selected Areas in Communications*, vol. 20, no. 3, pp. 561–569, 2002.
- [20] D. Reed, J. Smith, A. Rodriguez, and G. Calcev, "Spatial channel models for multi-antenna systems," in *Proceedings of the 58th IEEE Vehicular Technology Conference (VTC '03)*, vol. 1, pp. 99–103, Orlando, Fla, USA, October 2003.
- [21] P. Soma, D. S. Baum, V. Erceg, R. Krishnamoorthy, and A. J. Paulraj, "Analysis and modeling of multiple-input multiple-output (MIMO) radio channel based on outdoor measurements conducted at 2.5 GHz for fixed BWA applications," in *Proceedings of IEEE International Conference on Communications (ICC '02)*, vol. 1, pp. 272–276, New York, NY, USA, April–May 2002.
- [22] V. Erceg, H. Sampath, and S. Catreux-Erceg, "Dual-polarization versus single-polarization MIMO channel measurement results and modeling," *IEEE Transactions on Wireless Communications*, vol. 5, no. 1, pp. 28–33, 2006.
- [23] A. Pal, B. S. Lee, P. Rogers, G. Hilton, M. Beach, and A. Nix, "Effect of antenna element properties and array orientation on performance of MIMO systems," in *Proceedings of the 1st International Symposium on Wireless Communication Systems (ISWCS '04)*, pp. 120–124, Mauritius, September 2004.
- [24] B. S. Collins, "The effect of imperfect antenna cross-polar performance on the diversity gain of a dual-polarized receiving system," *Microwave Journal*, vol. 43, no. 4, pp. 84–94, 2000.